17th World Conference on Earthquake Engineering, 17WCEE
Sendai, Japan - September 13th to 18th 2020

COMPARISON OF FAULT PARAMETERS BETWEEN DYNAMIC AND STATIC MODELS OF INLAND CRUSTAL EARTHQUAKES

K. Irie[(1)], L. A. Dalguer[(2)], K. Dan[(3)], S. Dorjpalam[(4)],
D. Ju[(5)], H. Fujiwara [(6)], and N. Morikawa [(7)]

[(1)] *Principal Researcher, Ohsaki Research Institute, Inc., k.irie@ohsaki.co.jp*
[(2)] *Director, 3Q-Lab GmbH, luis.dalguer@3q-lab.ch*
[(3)] *Research Fellow, Ohsaki Research Institute, Inc., dan@ohsaki.co.jp*
[(4)] *Senior Research Engineer, Ohsaki Research Institute, Inc., saruul@ohsaki.co.jp*
[(5)] *Senior Research Engineer, Ohsaki Research Institute, Inc., judianshu@ohsaki.co.jp*
[(6)] *Principal Chief Researcher, National Research Institute for Earth Science and Disaster Resilience, Japan, fujiwara@bosai.go.jp*
[(7)] *Chief Researcher, National Research Institute for Earth Science and Disaster Resilience, Japan, morikawa@bosai.go.jp*

Abstract

In Japan, the procedure for setting an asperity model by the Headquarters for Earthquake Research Promotion (2017)[1], called Recipe, is often used in strong ground motion prediction for inland crustal earthquakes. In the Recipe, a circular crack formula is used to estimate the average stress drop of a seismic fault. However, when mega faults are considered and the fault length becomes longer, the circular crack formula cannot be applied, and fault parameters cannot be set. Irie *et al*. (2011)[2] and Irie *et al*. (2014)[3] have proposed approximate formulas to estimate the average dynamic stress drop for mega faults for vertical strike-slip faults and 60-degree dipping reverse faults using dynamic fault models with asperities. However, the agreement between the results of static fault models and those of the dynamic fault models has not been examined.

In this study, we calculated static slips using the parameters of the dynamic fault models for the vertical strike-slip faults (Irie *et al*., 2011[2]) and 60-degree dipping reverse faults (Irie *et al*., 2014[3]). Then we investigated the agreement between the seismic moments of the dynamic fault models and those of the static fault models.

In the dynamic faults by Irie *et al*. (2011)[2] and Irie *et al*. (2014)[3], the faults were set to rupture the ground surface. The fault width was 15 km for the vertical strike-slip faults and 17.4 km for the 60-degree dipping reverse faults assuming that the thickness of the seismogenic layer was 15 km. Eight patterns of the fault length varying from 15 to 300 km were studied. The number of the asperity was assumed to be one for each fault, and 5 patterns were considered by placing it at different locations. There were 2*8*5=80 fault models for these two fault types. The area of the asperity and the dynamic stress drop were determined by trial and error to fit the empirical relationships between the seismic moment and the fault area and that between the seismic moment and the short-period level. In the background, the dynamic stress drop was set to be 0 MPa.

In the static analyses of the fault models, the modified 3-D FDM code by Ely *et al*. (2008)[4] was used, and the dynamic stress drop was adopted as the static stress drop to calculate the slip. The geometry and the area of the asperity of the static fault models were set to be the same as those of the dynamic fault models.

The results of the static analyses of the vertical strike-slip faults showed that the slip of the static models was smaller than that of the dynamic models on almost the entire fault area. The seismic moments obtained by integrating the slip over the entire fault of the static models were 0.72 to 0.86 times of the seismic moments of the dynamic models, with average value of 0.76. On the other hand, the results of the static analyses of the 60-degree dipping reverse faults showed similar tendency to the vertical strike-slip faults in that the seismic moments calculated from the static analyses were smaller than those calculated from the dynamic analyses. However, differently from the vertical strike-slip faults, larger variations were observed between the static and dynamic results.

Keywords: static fault models, dynamic fault models, inland crustal earthquakes, seismic moment

1. Introduction

Asperity models are commonly used as source models for strong ground motion prediction in Japan. They are usually set according to the procedure, called Recipe, published by the Headquarters for Earthquake Research Promotion of Japan (2017)[1]. However, there are some instances when a valid asperity model is not attainable by the Recipe. For example, when a very long fault is considered, the Recipe will require a negative slip on the background area of the fault, which is not plausible in the kinematic fault model. This problem stems from the fact that the Recipe adopts the circular crack formula to calculate the stress drop for all types of faults, and that might not be applicable to very long faults with surface breakings. As a temporary solution, the Headquarters for Earthquake Research Promotion (2017)[1] suggested a value of 3.1 MPa for the average stress drop. The value of 3.1 MPa was derived by Fujii and Matsu'ura (2000)[5] for vertical strike-slip faults by applying the theoretical model of tectonic loading to the data of large intraplate strike-slip events. On the other hand, Irie *et al*. (2011)[2] proposed an approximate formula for average dynamic stress drop based on dynamic simulation results of vertical strike-slip faults with surface breakings, as an alternative for the circular crack formula. Moreover, Irie *et al*. (2014)[3] proposed an approximate formula for the average dynamic stress drop for 60-degree dipping reverse faults, following the same approach as in Irie *et al*. (2011)[2]. Nevertheless, the agreement of the results from dynamic and static analyses has not been examined yet.

Therefore, in this paper we investigated if the results from dynamic and static analyses agreed. For that, we carried out static analyses using dynamic models of Irie *et al*. (2011)[2] for vertical strike-slip faults and those of Irie *et al*. (2014)[3] for 60-degree dipping reverse faults, and compared the seismic moments and the geometric stress drop shape factors obtained from both the dynamic and static analyses.

2. Static Solution for Vertical Strike-Slip Faults

2.1 Geometric dynamic stress drop shape factor for vertical strike-slip faults by Irie *et al*. (2011)[2]

Irie *et al*. (2011)[2] set up dynamic vertical strike-slip fault models with surface breakings, which would follow the accepted empirical relationships between the seismic moment and the fault area and the empirical relationship between the seismic moment and the short-period level for crustal earthquakes. Then, geometric dynamic stress drop shape factors c_D were calculated from Eq. (1).

$$\Delta\sigma^{\#} = c_D \, [M_{0D} / (L W_{max}^2)] \tag{1}$$

Here, $\Delta\sigma^{\#}$ is the dynamic stress drop, c_D is the geometric dynamic stress drop shape factor, M_{0D} is the seismic moment calculated from the final slip distribution results by the dynamic simulations, L is the fault length, and W_{max} is the fault width. The fault models used in the dynamic simulations were of rectangular shape reaching the ground surface, with 15-km width and eight different lengths of 15, 20, 25, 30, 35, 50, 100, and 300 km. One asperity was set for each fault model with five different location patterns (top left, bottom left, center, top center, and bottom center of the fault plane). Thereby, there were 40 different fault models in total. The fault plane was embedded in a uniform material with *S*-wave velocity of Vs=3.5 km/s, *P*-wave velocity of Vp=6.0 km/s, and density of ρ=2.7 t/m^3. Based on the simulation results, they obtained the approximate formula for the geometric dynamic stress drop shape factor expressed in terms of the fault aspect ratio (L/W) as follows:

$$c_D = 0.5 + 2 \exp[-L / W_{max}]. \tag{2}$$

2.2 Static analyses of vertical strike-slip faults

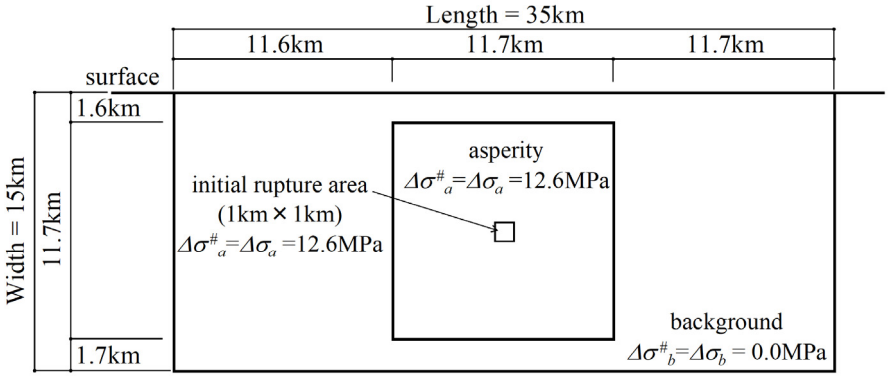

Fig. 1 – Example of vertical strike-slip fault models (L=35km, asperity at the center)

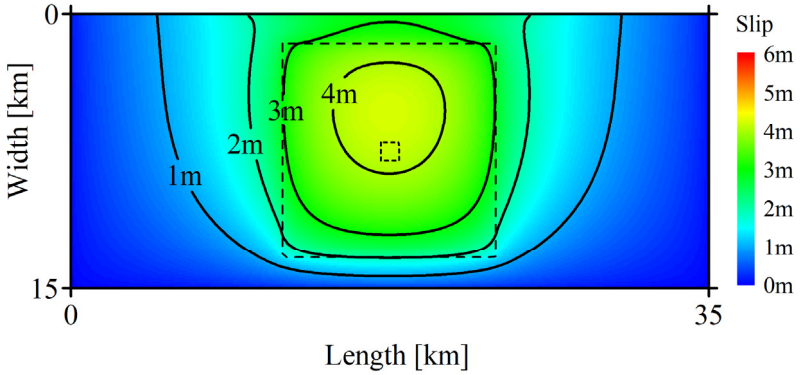

Fig. 2 – Example of the static analysis results for the vertical strike-slip faults (fault model depicted in Fig.1)

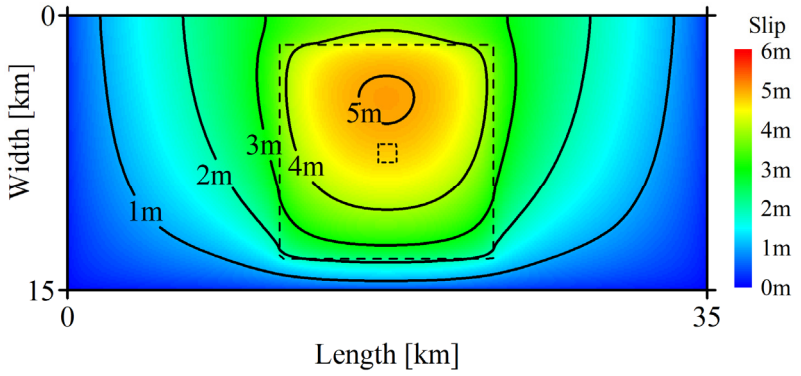

Fig. 3 – Example of the dynamic analysis results for the vertical strike-slip faults (fault model depicted in Fig.1) 【From Irie *et al.* (2011)[2]】

For the static analyses of this paper, we used 40 fault models of the same geomety (fault size, asperity size, and asperity location) as in Irie *et al.* (2011)[2]. For static stress drop of each model, we adopted the value of the dynamic stress drop in Irie *et al.* (2011)[2]. We performed the calculations using the Finite Difference Method Code by Ely *et al.* (2008)[4], which was modified to evaluate only static deformation. Initially, the faults were excited dynamically with impulsive input of stress drop, and then the propagated waves were dumped leaving the static deformation.

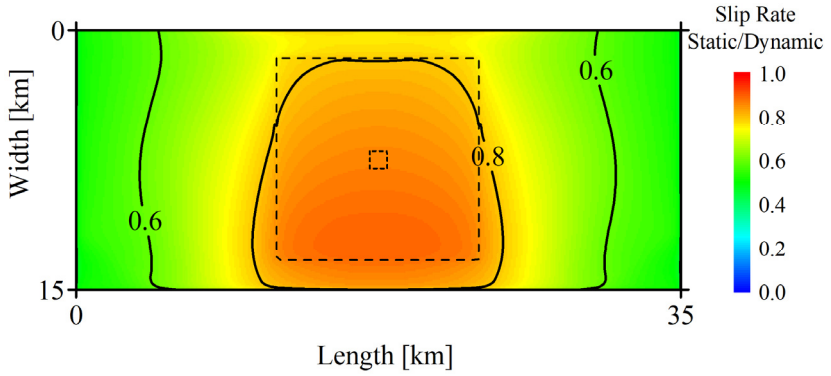

Fig. 4 – Example of the ratios of the slip by the static analyses to that by the dynamic analyses for the vertical strike-slip faults (fault model depicted in Fig.1)

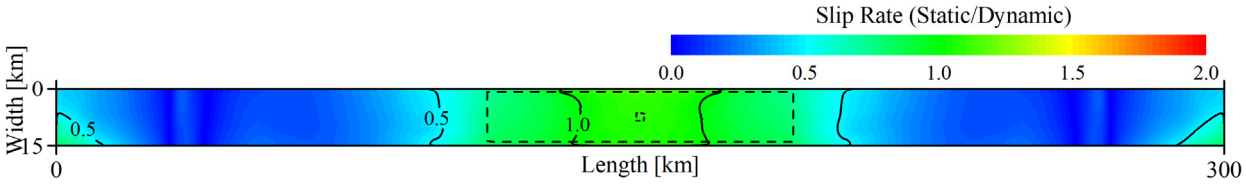

Fig. 5 – Example of the ratios of the slip by the static analyses to that by the dynamic analyses for the vertical strike-slip faults (L=300km, asperity at the center)

An example of the fault models and its static analysis result are shown in Fig.1 and Fig.2, respectively. For reference, the dynamic result for the same fault model is shown in Fig.3. The trends in the slip distribution from the static analysis (Fig.2) and the final slip distribution from the dynamic analysis (Fig.3) are similar, although the static analysis slip is slightly smaller. Also, in Fig.4 we examine the difference between the static and dynamic final slip distributions in terms of the static to dynamic result ratio. The ratio is relatively larger on the asperity decreasing with the distance away from the asperity, and it is lower than 1 on the entire fault. This tendency of the slip ratio is more prominent when the fault grows longer, with the ratio even exceeding 1 in the center of the asperity for the 300-km long fault models as shown in Fig.5.

The parameters of all the forty vertical strike-slip fault models are compiled in Table 1. Furthermore, the seismic moments computed from the static and dynamic analysis results are compared in Fig.6. From Table 1 and Fig.6, we retrieve the seismic moment ratios to be 0.72～0.86 (with arithmetic mean of 0.76), which shows that the the ratios are quite consistent for all the fault models.

Next, in Eq. (1) we replaced $\Delta\sigma^{\#}$ with the average static stress drops $\Delta\sigma$ and M_{0D} with the seismic moments M_{0S} computed from the static results, and then calculated the geometric static stress drop shape factors c_S as expressed by the following equation:

$$\Delta\sigma = c_S \, [M_{0S} / (L W_{max}^2)]. \tag{3}$$

In Fig.7, we plotted the geometric static stress drop shape factors for all the models against the fault aspect ratios. For reference, we added the data of the geometric dynamic stress drop shape factors and the approximate formula that fits the data from Irie *et al.* (2011)[2], as well as the geometric static stress drop shape factor curve derived by Hikima and Shimmura (2018)[6]. Furthermore, from Fig.7 it is clear that the geometric static stress drop shape factors are larger than the geometric dynamic stress drop shape factors and that they agree well with the geometric static stress drop shape factor curve derived by Hikima and Shimmura (2018)[6].

Table 1 – Fault model parameters for the vertical strike-slip faults

Fault Model	Input Parameters						Dynamic Analyses Results (Irie *et al*., 2011)		Static Analyses Results (this study)			
	Asperity Location	Fault Length L [km]	Fault Width W [km]	Asperity Area S_a [km^2]	Stress Drop on Asperity $\Delta\sigma^{\#}{}_a$ [MPa]	Average Stress Drop $\Delta\sigma^{\#}$[MPa]	Seismic Moment (computed from final slip distribution) M_{0D} [N·m]	Geom. Stress Drop Shape Factor c_D	Seismic Momet (computed from slip distribution) M_{0S} [N·m]	M_{0S}/M_{0D}	Geom. Stress Drop Shape Factor c_S	c_S/c_D
SL15M1	Top Left	15	15	64.00	12.0	3.41	9.16E+18	1.26	6.71E+18	0.73	1.72	1.36
SL20M1		20	15	86.49	11.9	3.43	1.47E+19	1.05	1.08E+19	0.74	1.43	1.36
SL25M1		25	15	121.00	11.3	3.65	2.18E+19	0.94	1.61E+19	0.74	1.27	1.35
SL30M1		30	15	169.00	10.4	3.91	2.97E+19	0.89	2.23E+19	0.75	1.18	1.33
SL35M1		35	15	212.80	10.1	4.09	3.86E+19	0.84	2.90E+19	0.75	1.11	1.33
SL50M1		50	15	308.00	10.1	4.15	6.77E+19	0.69	5.07E+19	0.75	0.92	1.34
SL100M1		100	15	551.60	10.6	3.90	1.55E+20	0.57	1.21E+20	0.78	0.72	1.28
SL300M1		300	15	1391.60	11.6	3.59	4.67E+20	0.52	3.97E+20	0.85	0.61	1.18
SL15M2	Bottom Left	15	15	96.04	9.8	4.18	9.20E+18	1.53	6.88E+18	0.75	2.05	1.34
SL20M2		20	15	125.44	9.9	4.14	1.48E+19	1.26	1.12E+19	0.76	1.66	1.32
SL25M2		25	15	158.76	9.9	4.19	2.16E+19	1.09	1.64E+19	0.76	1.44	1.32
SL30M2		30	15	197.40	9.7	4.26	2.98E+19	0.96	2.26E+19	0.76	1.27	1.32
SL35M2		35	15	235.20	9.6	4.30	3.86E+19	0.88	2.94E+19	0.76	1.15	1.31
SL50M2		50	15	345.80	9.5	4.38	6.76E+19	0.73	5.17E+19	0.76	0.95	1.31
SL100M2		100	15	621.60	10.0	4.14	1.55E+20	0.60	1.23E+20	0.80	0.76	1.26
SL300M2		300	15	1604.40	10.8	3.85	4.66E+20	0.56	4.00E+20	0.86	0.65	1.16
SL15M3	Center	15	15	53.29	13.1	3.10	9.18E+18	1.14	6.92E+18	0.75	1.51	1.33
SL20M3		20	15	67.24	13.5	3.03	1.48E+19	0.92	1.12E+19	0.76	1.22	1.32
SL25M3		25	15	86.49	13.3	3.07	2.17E+19	0.79	1.64E+19	0.76	1.05	1.32
SL30M3		30	15	110.25	12.9	3.16	2.97E+19	0.72	2.26E+19	0.76	0.94	1.31
SL35M3		35	15	136.89	12.6	3.29	3.88E+19	0.67	2.96E+19	0.76	0.87	1.31
SL50M3		50	15	217.10	11.9	3.44	6.75E+19	0.57	5.17E+19	0.77	0.75	1.31
SL100M3		100	15	369.20	13.0	3.20	1.55E+20	0.46	1.17E+20	0.75	0.62	1.33
SL300M3		300	15	1021.80	13.5	3.07	4.67E+20	0.44	3.70E+20	0.79	0.56	1.26
SL15M4	Top Center	15	15	40.96	15.0	2.73	9.16E+18	1.01	6.59E+18	0.72	1.40	1.39
SL20M4		20	15	51.84	15.3	2.64	1.48E+19	0.81	1.07E+19	0.72	1.11	1.38
SL25M4		25	15	67.24	15.1	2.71	2.18E+19	0.70	1.60E+19	0.73	0.95	1.37
SL30M4		30	15	84.64	14.7	2.76	2.96E+19	0.63	2.18E+19	0.74	0.86	1.36
SL35M4		35	15	108.16	14.1	2.90	3.86E+19	0.59	2.86E+19	0.74	0.80	1.35
SL50M4		50	15	204.40	12.3	3.35	6.76E+19	0.56	5.11E+19	0.76	0.74	1.32
SL100M4		100	15	345.80	13.4	3.09	1.55E+20	0.45	1.15E+20	0.74	0.60	1.35
SL300M4		300	15	942.20	14.1	2.95	4.67E+20	0.43	3.66E+20	0.78	0.54	1.28
SL15M5	Bottom Center	15	15	79.21	10.7	3.77	9.15E+18	1.39	6.79E+18	0.74	1.87	1.35
SL20M5		20	15	96.04	11.3	3.62	1.47E+19	1.10	1.11E+19	0.75	1.47	1.33
SL25M5		25	15	118.81	11.4	3.61	2.16E+19	0.94	1.65E+19	0.76	1.23	1.31
SL30M5		30	15	144.00	11.3	3.62	2.96E+19	0.82	2.29E+19	0.77	1.07	1.29
SL35M5		35	15	169.00	11.3	3.64	3.88E+19	0.74	3.00E+19	0.77	0.95	1.29
SL50M5		50	15	242.20	11.3	3.65	6.76E+19	0.61	5.19E+19	0.77	0.79	1.30
SL100M5		100	15	417.20	12.2	3.39	1.55E+20	0.49	1.18E+20	0.76	0.65	1.31
SL300M5		300	15	1142.40	12.8	3.25	4.67E+20	0.47	3.71E+20	0.79	0.59	1.26

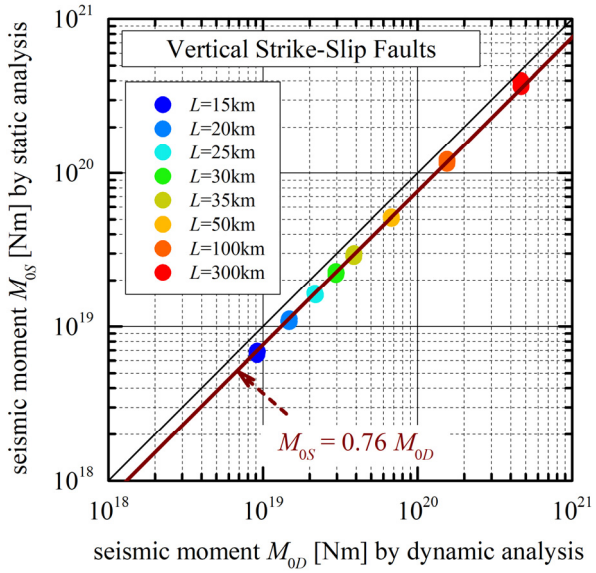

Fig. 6 – Comparison of the seismic moment by static analyses and those by dynamic analyses for the vertical strike-slip faults

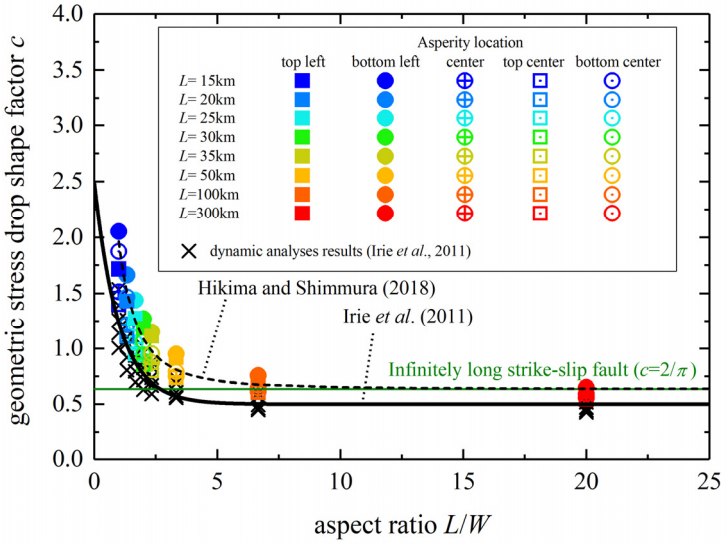

Fig. 7 – The geometric static stress drop shape factors for the vertical strike-slip faults calculated from the static analysis results

We compared the dynamic and static geometric stress drop shape factors for all the fault models in Fig.8. There is a clear general trend for all the fault models, and the mean ratio of the geometric static stress drop shape factors to the geometric dynamic ones is 1.31, which is also the reciprocal of the ratio of the seismic moments by the dynamic analyses to those by the static analyses.

3. Static Solution for 60-degree Dipping Reverse Faults

3.1 Geometric dynamic stress drop shape factor for 60-degree dipping reverse faults by Irie *et al.*(2014)[3]

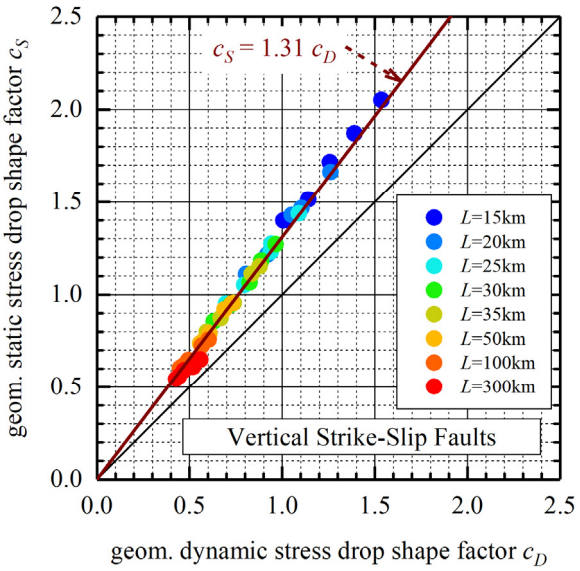

Fig. 8 – Comparison of the static and dynamic geometric stress drop shape factors for the vertical strike-slip faults

Irie *et al.* (2014)[3] have conducted the same studies as described in 2.1 for 60-degree dipping reservse faults with surface breakings. The fault models used in the dynamic simulations were of rectangular shapes reaching the ground surface, with 17.4-km width and eight different lengths of 15, 20, 25, 30, 35, 50, 100, and 300 km. One asperity was set for each fault model with five different location patterns (top-left, bottom-left, center, top center, and bottom center of the fault plane). Thereby, there were 40 different fault models in total. Based on the simulation results, they obtained the approximate formula for the geometric dynamic stress drop shape factor expressed in terms of the fault aspect ratio (L/W) for 60-degree dipping reverse faults as shown in Eq. (4).

$$c_D = 0.45 + 0.7 \exp[-L / W_{max}] \tag{4}$$

3.2 Static analyses of 60-degree dipping reverse faults

For the static analyses in this paper, we used 40 fault models of the same geomety (fault size, asperity size, and asperity location) as in Irie *et al.* (2014)[2]. For static stress drop of each model, we adopted the value of the dynamic stress drop in Irie *et al.* (2014)[2]. The calculations were performed using the same code as described in 2.2.

An example of the 60-degree dipping reverse fault models and its static analysis result are shown in Fig.9 and Fig.10, respectively. For reference, the dynamic result for the same fault model is shown in Fig.11. The slip from the static analysis (Fig.10) is in overall smaller than the slip from the dynamic analysis (Fig.11). However, the slip near the surface is larger in the static results compared to the dynamic results. Also, in Fig.12 we compare the slip by the static analysis and that by the dynamic analysis in terms of the static to dynamic result ratio distributed over the fault plane. On this distribution plot, the ratio exceeds 1 near the ground surface above the asperity, which means that the slip computed statically is larger than that computed dynamically, and the ratio decreases with the distance away from the asperity. This distribution pattern is more prominent when the fault lenght becomes longer. For example, in case of the 300-km long fault model the ratio on the asperity is 1 to 1.5 as shown in Fig.13.

The parameters of all the forty 60-degree dipping reverse fault models are compiled in Table 2. Furthermore, the seismic moments computed from the static and dynamic slip distribution results are

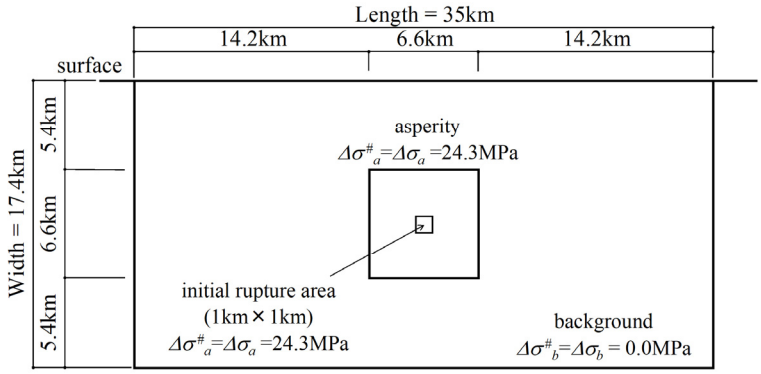

Fig. 9 – Example of the 60-degree reverse fault models (L=35km, asperity at the center)

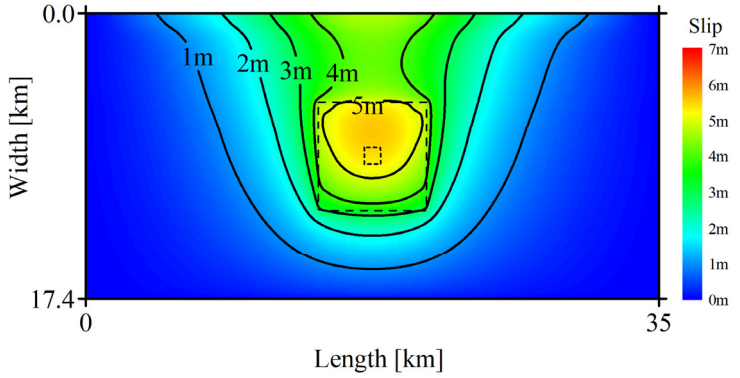

Fig. 10 – Example of the static analysis results for the 60-degree reverse faults (fault model depicted in Fig.9)

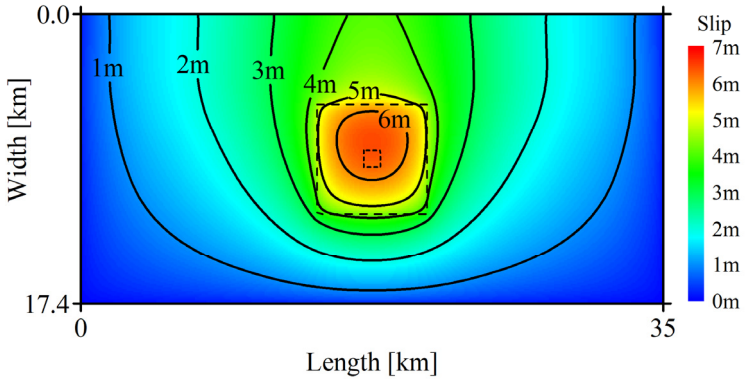

Fig. 11 – Example of the dynamic analysis results for the 60-degree reverse faults (fault model depicted in Fig.9) 【From Irie *et al.* (2014)[3]】

compared in Fig.14. Although there is an area around the asperity top (Fig.12), where the slip by the static analysis is larger than the slip by the dynamic analysis, the entire seismic moment ratios in Table 2 and Fig.14 are less than one, which indicates that the seismic moments from the static analyses are smaller than those from the dynamic analyses. The ratios of the seismic moments by the static analyses to those by the dynamic analyses for the fault models shorter than 50 km are between 0.61 to 0.72, which are relatively smaller than the ratios for the vertical strike-slip faults (Table 1 and Fig.6). However, the ratios of the

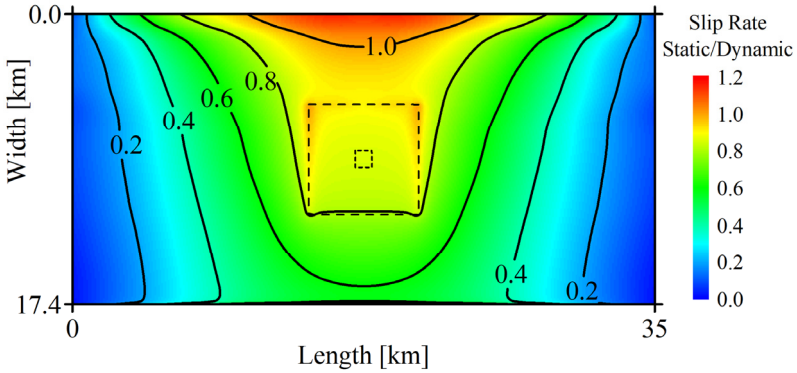

Fig. 12 – Example of the ratio of the slip by the static analysis to that by dynamic analysis for the 60-degree reverse faults (fault model depicted in Fig.9)

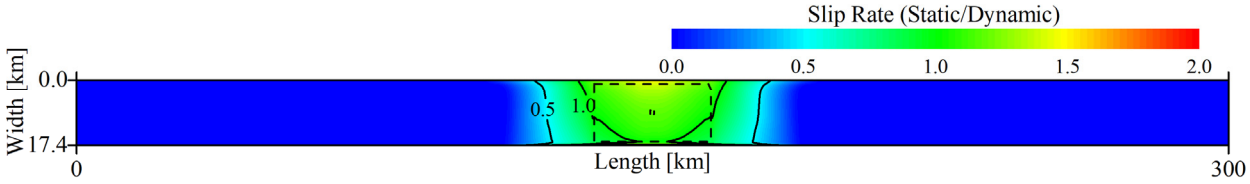

Fig. 13 – Example of the ratio of the slip by the static analysis to that by dynamic analysis for the 60-degree reverse faults (L=300km, asperity at the center)

seismic moments for the fault models longer than 100 km noticeably increase to 0.79 to 0.96, which are greater than the ratios for the vertical strike-slip faults (Table 1 and Fig.6). The arithmetic average of all the reverse fault models is 0.73.

Similarly to the vertical strike-slip fault models, we calculated the geometric static stress drop shape factors c_S for the 60-degree dipping reverse fault models using Eq. (3) and plotted the geometric static stress drop shape factors for all the models against fault aspect ratios in Fig.15. On the plot, the geometric dynamic stress drop shape factor data and the approximate formula that fits the data from Irie *et al.* (2014)[3] is added for reference. From Fig.15 it is clear that the geometric static stress drop shape factors are greater than the geometric dynamic stress drop shape factors, although for the fault models with the lengths longer than 100 km the values are similar. We compared the dynamic and static geometric stress drop shape factors for all the fault models in Fig.16. The mean ratio of the static to dynamic geometric stress drop shape factors is 1.31, but the results are more scattered than the corresponding plots for the vertical strike-slip fault models (Fig.8). Furthermore, in Fig.16 there is a threshold at fault length between 50km and 100km, where the correlation trends are changing.

4. Conclusions

We carried out static analyses of the vertical strike-slip and 60-degree dipping reverse fault models loaded with the static stress drop of the same value as the dynamic stress drops of the same fault models as in the dynamic analyses of Irie *et al.* (2011)[2] and Irie *et al.* (2014)[3], and then compared the static and dynamic results. For the vertical strike-slip faults, the trends in the slip distribution of the static analyses and the final slip distribution of the dynamic analyses were similar, although the slip (seismic moment) from the static analyses were smaller (0.76 fold in average) than those from the dynamic results. The difference could be caused by the overshooting effect in the dynamic analyses. Also, the geometric static stress drop shape factors calculated from the static analyses were about 1.31 greater than those from the dynamic analyses.

Table 2 – Fault model parameters for the 60-degree dipping reverse faults

Fault Model	Input Parameter						Dynamic Analyses Results (Irie *et al*., 2014)		Static Analyses Results (this study)			
	Asperity Location	Fault Length L [km]	Fault Width W [km]	Asperity Area S_a [km^2]	Stress Drop on Asperity $\Delta\sigma^{\#}_a$ [MPa]	Average Stress Drop $\Delta\sigma^{\#}$ [MPa]	Seismic Moment (computed from final slip distribution) M_{0D} [N·m]	Geom. Stress Drop Shape Factor c_D	Seismic Momet (computed from slip distribution) M_{0S} [N·m]	M_{0S}/M_{0D}	Geom. Stress Drop Shape Factor c_S	c_S/c_D
RL15M1	Top Left	15	17.4	24.01	21.4	1.97	1.14E+19	0.78	7.97E+18	0.70	1.12	1.43
RL20M1		20	17.4	31.36	21.9	1.97	1.77E+19	0.67	1.20E+19	0.68	1.00	1.48
RL25M1		25	17.4	42.25	20.8	2.02	2.50E+19	0.61	1.63E+19	0.65	0.94	1.53
RL30M1		30	17.4	54.76	20.0	2.10	3.33E+19	0.57	2.15E+19	0.65	0.89	1.55
RL35M1		35	17.4	67.24	19.7	2.18	4.23E+19	0.55	2.72E+19	0.64	0.85	1.55
RL50M1		50	17.4	116.64	17.9	2.40	7.14E+19	0.51	5.13E+19	0.72	0.71	1.39
RL100M1		100	17.4	318.16	15.4	2.82	1.64E+20	0.52	1.50E+20	0.92	0.57	1.09
RL300M1		300	17.4	747.84	17.3	2.48	4.95E+20	0.45	4.59E+20	0.93	0.49	1.08
RL15M2	Bottom Left	15	17.4	73.96	12.3	3.49	1.16E+19	1.36	8.25E+18	0.71	1.92	1.41
RL20M2		20	17.4	84.64	13.2	3.21	1.77E+19	1.10	1.21E+19	0.68	1.61	1.46
RL25M2		25	17.4	98.01	13.9	3.13	2.51E+19	0.94	1.67E+19	0.67	1.42	1.50
RL30M2		30	17.4	116.64	13.8	3.08	3.34E+19	0.84	2.23E+19	0.67	1.26	1.50
RL35M2		35	17.4	132.25	14.1	3.06	4.22E+19	0.77	2.90E+19	0.69	1.12	1.46
RL50M2		50	17.4	184.96	14.4	3.06	7.14E+19	0.65	5.64E+19	0.79	0.82	1.27
RL100M2		100	17.4	346.04	14.8	2.94	1.64E+20	0.54	1.53E+20	0.93	0.58	1.07
RL300M2		300	17.4	816.72	16.6	2.60	4.95E+20	0.48	4.77E+20	0.96	0.49	1.04
RL15M3	Center	15	17.4	23.04	21.8	1.92	1.16E+19	0.76	7.97E+18	0.69	1.10	1.45
RL20M3		20	17.4	25.00	24.2	1.74	1.77E+19	0.59	1.27E+19	0.72	0.83	1.40
RL25M3		25	17.4	29.16	25.2	1.69	2.50E+19	0.51	1.74E+19	0.70	0.73	1.44
RL30M3		30	17.4	36.00	24.8	1.71	3.34E+19	0.47	2.28E+19	0.68	0.68	1.46
RL35M3		35	17.4	43.56	24.3	1.74	4.24E+19	0.43	2.88E+19	0.68	0.64	1.47
RL50M3		50	17.4	65.61	23.9	1.80	7.15E+19	0.38	5.01E+19	0.70	0.54	1.43
RL100M3		100	17.4	139.24	23.2	1.86	1.63E+20	0.34	1.42E+20	0.87	0.40	1.15
RL300M3		300	17.4	468.16	21.9	1.96	4.95E+20	0.36	4.22E+20	0.85	0.42	1.17
RL15M4	Top Center	15	17.4	13.69	28.1	1.47	1.16E+19	0.58	8.23E+18	0.71	0.81	1.41
RL20M4		20	17.4	16.81	29.3	1.42	1.77E+19	0.48	1.23E+19	0.69	0.70	1.44
RL25M4		25	17.4	21.16	29.3	1.43	2.50E+19	0.43	1.65E+19	0.66	0.65	1.52
RL30M4		30	17.4	26.01	29.2	1.45	3.32E+19	0.40	2.08E+19	0.63	0.64	1.60
RL35M4		35	17.4	32.49	28.1	1.50	4.24E+19	0.38	2.59E+19	0.61	0.61	1.64
RL50M4		50	17.4	51.84	26.7	1.59	7.16E+19	0.34	4.34E+19	0.61	0.55	1.65
RL100M4		100	17.4	110.25	26.1	1.65	1.64E+20	0.30	1.30E+20	0.79	0.39	1.26
RL300M4		300	17.4	469.04	21.9	1.97	4.96E+20	0.36	4.16E+20	0.84	0.43	1.19
RL15M5	Bottom Center	15	17.4	59.29	13.7	3.11	1.15E+19	1.22	8.11E+18	0.70	1.74	1.42
RL20M5		20	17.4	62.41	15.4	2.76	1.77E+19	0.94	1.16E+19	0.65	1.44	1.53
RL25M5		25	17.4	68.89	16.5	2.61	2.51E+19	0.79	1.62E+19	0.65	1.22	1.55
RL30M5		30	17.4	77.44	17.1	2.54	3.33E+19	0.69	2.11E+19	0.63	1.09	1.58
RL35M5		35	17.4	88.36	17.2	2.50	4.24E+19	0.62	2.81E+19	0.66	0.94	1.51
RL50M5		50	17.4	116.64	18.1	2.43	7.16E+19	0.51	5.15E+19	0.72	0.71	1.39
RL100M5		100	17.4	196.00	19.6	2.21	1.64E+20	0.41	1.46E+20	0.89	0.46	1.13
RL300M5		300	17.4	518.24	20.8	2.07	4.94E+20	0.38	4.23E+20	0.86	0.44	1.17

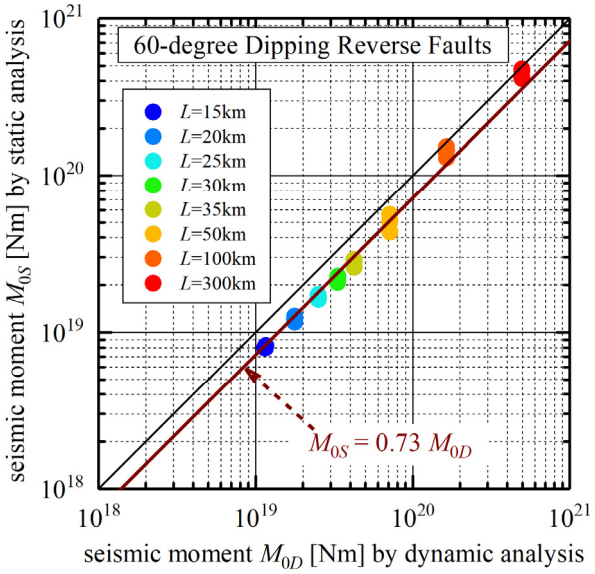

Fig. 14 – Comparison of the seismic moments by the static analyses with those by the dynamic analyses results for the 60-degree dipping reverse faults

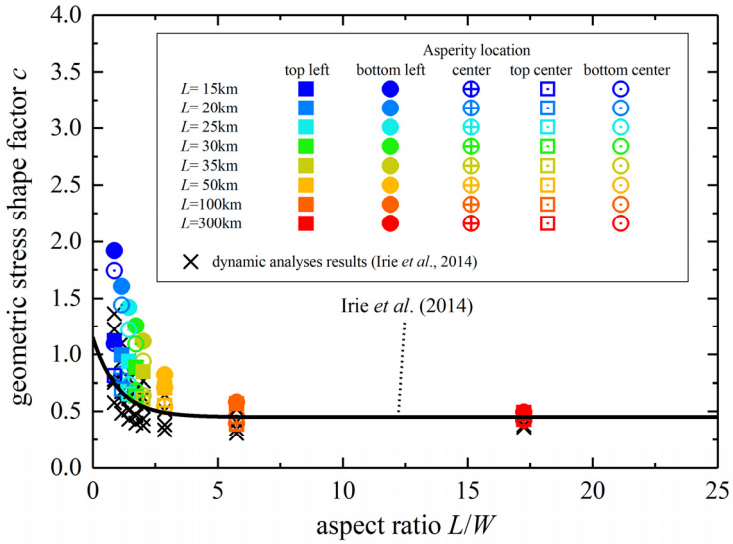

Fig. 15 – The geometric static stress drop shape factors for the 60-degree dipping reverse faults calculated from the static analysis results

As for the 60-degree dipping reverse faults, similarly to the vertical strike-slip faults, the seismic moments calculated from the static analyses were smaller than those calculated from the dynamic analyses, although the slip near the ground surface above the asperity was greater for the static analyses. Furthermore, the correlation plots of the dynamic and static comparison were scattered more than those for the vertical strike-slip faults, and a clear correlation could not be established. The cause for the indistinct correlation for the reverse fault models could lie in the dipping of the fault plane, or in the direction of slip towards the ground surface, or other factors. Further study might be necessary to examine those causes.

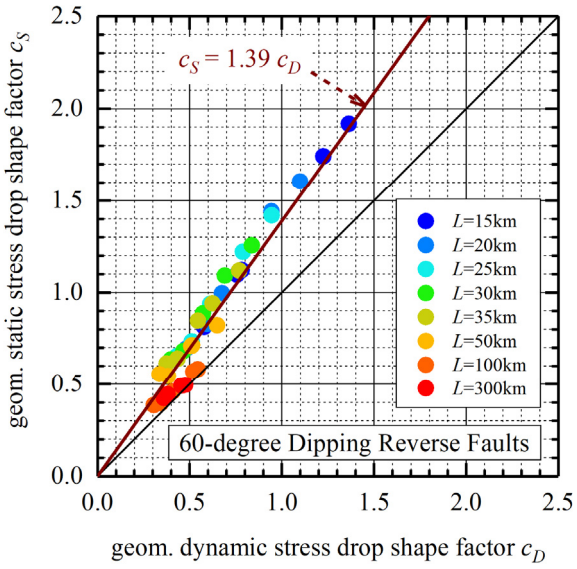

Fig. 16 – Comparison of the static and dynamic geometric stress drop shape factors for the 60-degree dipping reverse faults

5. Acknowledgements

The dynamic study of the 60-degree dipping reverse faults is part of the research project funded by the Secretariat of the Nuclear Regulation Authority (NRA), Japan, in fiscal year 2013. The static study of the 60-degree dipping reverse faults is part of the research project funded by the National Research Institute for Earth Science and Disaster Resilience of Japan in fiscal year of 2019.

6. References

[1] Headquarters for Earthquake Research Promotion (2017): *Strong ground motion prediction method for earthquakes with specified source faults ("Recipe")*. (in Japanese)

[2] Irie K, Dan K, Dorjpalam S, Kawasato T, Ikutama S, Irikura K (2011): Procedure for establishing asperity models for long strike-slip faults based on change in scaling laws of fault parameters. Part 3: Estimation of the formula for average dynamic stress drop by dynamic rupturing simulation. *Summaries of technical papers of annual meeting AIJ*, 21052, 103-104. (in Japanese)

[3] Irie K, Dan K, Ju D, Shimazu N, Torita H (2014): Estimation of averaged dynamic stress drops of inland earthquakes caused by long reverse faults and its application to prediction of strong ground motions. Part 1: Examination of geometrical constant for dynamic stress drop. *Summaries of technical papers of annual meeting AIJ*, 21107, 213-214. (in Japanese)

[4] Ely G P, Steven M D, Jean-Bernard M (2008): A support-operator method for viscoelastic wave modelling in 3-D heterogeneous media. *Geophysical. Journal. International*, **172**, 331-344.

[5] Fujii Y, Matsu'ura M (2000): Regional difference in scaling laws for large earthquakes and its tectonic implication. *Pure and Applied Geophysics*, **157**, 2283-2302.

[6] Hikima K, Shimmura A (2018): Moment-area assuming constant stress drop from medium to great crustal earthquake -Part 1-. *Summaries of Technical Papers of Annual Meeting AIJ*, 21388, 775-776. (in Japanese)

